第21卷第5期　　红外与毫米波学报　　Vol. 21, No. 5
2002年10月　　J. Infrared Millim. Waves　　October, 2002

QUANTUM MECHANICAL MODEL AND SIMULATION OF GaAs/AlGaAs QUANTUM WELL INFRARED PHOTODETECTOR-Ⅰ OPTICAL ASPECTS

Fu Y　Willander M
(Physical Electronics and Photonics, Microtechnology Center at Chalmers, Department of Microelectronics and Nanoscience, Chalmers University of Technology, Fysikgränd 3, S-412 96 Gothenburg, Sweden)
Li Ning　Lu W
(National Laboratory for Infrared Physics, Shanghai Institute of Technical Physics, Chinese Academy of Sciences, 500 Yu-Tian Road, Shanghai 200083, China)

Abstract　A complete quantum mechanical model for GaAs/AlGaAs quantum well infrared photodetectors (QWIPs) is presented here. The model consisted of four parts: (1) Starting with the description of the electromagnetic field of the infrared radiation in the QWIP, effective component of the vector potential $\langle|A_z|\rangle$ along the QWIP growth direction (z-axis) due to the optical diffraction grating was calculated. (2) From the wave transmissions and the occupations of the electronic states, it was discussed that the dark current in the QWIP is determined by the drift-diffusion current of carriers thermally excited from the ground sublevel in the quantum well to extended states above the barrier. (3) The photocurrent was investigated by the optical transition (absorption coefficient between the ground state to excited states due to the nonzero $\langle|A_z|\rangle$). (4) By studying the inter-diffusion of the Al atoms across the GaAs/AlGaAs heterointerfaces, the mobility of the drift-diffusion carriers in the excited states was calculated, so the measurement results of the dark current and photocurrent spectra can be explained theoretically. With the complete quantum mechanical descriptions of (1-4), QWIP device design and optimization are possible.
Key words　GaAs/AlGaAs, photodetector, quantum well infrared photodetector (QWIP), quantum mechanical model.

Introduction

Infrared detector technique has been a key factor in the development of the infrared technology for more than 40 years. Since 1970, semiconductors like InSb and HgCdTe have been the principal materials for various infrared detector applications. The format of the infrared detector motivated by smart thermal imaging system changed from single element device to focal plan arrays (FPAs) in the middle of 80's [1]. Today's technology of infrared detector concentrates largely on focal plan arrays, expecially for sensitive, homogeneous and large format scale devices.

HgCdTe has been recognized as the most important semiconductor alloy for infrared detector because of its direct energy band gap which can be tuned to infrared radiation wavelength of interest [2]. Long-wavelength infrared detectors have been very well developed on the HgCdTe materials with background limited performance at about 100 K for terrestrial application. However the development of large format FPA and very long wavelength HgCdTe detectors is limited by the instabilities in the lattices, surfaces and interfaces of HgCdTe-based materials and devices.

Due to the rapid development of low-dimensional materials, the quantum well infrared photodetector (QWIP) has been exploring in a flourishing manner in the past decade [3-5] and the research activities in

Received 2001-03-11, revised 2002-09-17
稿件收到日期2001-03-11,修改稿收到日期2002-09-17

this field have been very dynamic. A 9-μm cutoff 640 ×486 snap-shot quantum well infrared photodetector camera was demonstrated with a noise equivalent differential temperature of 36mK [3]. A lot of investigations have been concentrated on the comparison between HgCdTe and QWIP detectors [2,6,7] and it has been generally concluded that the GaAs/AlGaAs multiple quantum well photodetector is very promising for long-wavelength applications. Compared with HgCdTe photodiodes, the GaAs/AlGaAs QWIPs have their advantages in large uniform FPAs, mature Ⅲ-Ⅴ technology, high production yield, low cost, high speed, radiation hardness and very long wavelength availability. However, in the thermal image application, the QWIPs are limited by low quantum efficiency, high dark current and narrow spectral bandwidth. They also require either non-normal radiation incidence or optical grating for optical coupling.

Like any other electronic and optoelectronic devices, the device modeling has always been an important issue in the infrared detector design and fabrication. There have been quite a lot of works on the semiclassical model about HgCdTe devices based on the Poisson equation, the transport and continuum equations[1,8-10]. A practical model about the QWIP is expected to be able to predicate essential electrical and optical properties of the QWIP.

Various physical aspects about the QWIP has been well studied, including the special behaviors on electron-electron and electron-phonon interactions, intersubband transitions, optical coupling and electron transport[11]. It is of vital importance however to establish a practical device model, including all essential properties of the QWIP to design and to optimize its device performances. Since the fabrication process of a Ⅲ-Ⅴ-based QWIP is much mature than the conventional HgCdTe and InSb infrared detectors, the QWIP does not have so much uncontrolled factors induced during the device fabrication processes (Lattice, surface and interface instabilities in HgCdTe). Thus a physical QWIP model could be at first sight easier to realize. However it is proved that the theoretical treatment of the QWIP is more complicated than that of HgCdTe due to two principal reasons.

The first one is the comparable sizes of the thickness of the optical active layer and the wavelength of the infrared radiation. In addition there exists a metal-semiconductor interface in thin active layer of a real QWIP device. The physical model has to treat the lossy QWIP material including the near field effect [12,13]. Secondly the QWIP model involves the quantum mechanical description of the optical excitation and the semiclassical carrier transport [14]. In the conventional HgCdTe and InSb infrared detectors, the optical active layer is much thicker than the wavelength of the infrared radiation and the carrier coherence length so that quantum mechanical effect is not important.

Here we try to establish a practical GaAs/AlGaAs QWIP model based on the real device structures. The first part deals with the optical aspects and the second part the electrical aspects.

1 General consideration of optical transition

Denoting the electronic state by its quantum number k and the photon state by photon energy $\hbar\omega$ and photon density n_{ph}, the absorption rate between two electronic states k_i and k_j is[15]

$$W_{ij}(\hbar\omega)=\frac{\pi\hbar^2e^2n_{ph}}{m_0^2\omega\varepsilon}|\langle k_j|\ a\cdot p\ |k_i\rangle|^2\delta[E(k_j)-E(k_j)+\hbar\omega]. \quad (1)$$

where $|k_j\rangle$ and $E(k_i)$ are, respectively, the wavefunction and eigenvalue of state k_i. The net absorption rate (per unit time) of the system in a photon field is calculated by

$$W(\hbar\omega)=\sum_{ji}W_{ji}(\hbar\omega)\{f[E(k_i)]-f[E(k_j)]\}, \quad (2)$$

where $f[E(k_j)]$ and $f[E(k_i)]$ are occupations of the final and initial electronic states, introduced here due to the Pauli exclusion principle (the initial state occupied and the final state empty).

We consider a beam of photons traveling along the z-axis, we can write the continuity equation for the photon density

$$\frac{dn_{ph}(\hbar\omega,z)}{dt}=\frac{\partial n_{ph}(\hbar\omega,z)}{\partial t}-\frac{\partial[vn_{ph}(\hbar\omega,z)]}{\partial z}, \quad (3)$$

where the first term on the right side of the above equation represents the absorption rate of photons and

the second term represents the photons leaving due to the photon current. At the steady state of $dn_{ph}(\hbar\omega, z)/dt = 0$, we have

$$n_{ph}(\hbar\omega, z) = n_0(\hbar\omega)\, e^{-\alpha(\hbar\omega) z}, \quad (4)$$

which defines the absorption coefficient $\alpha(\hbar\omega)$. Since

$$\frac{\partial n_{ph}(\hbar\omega, z)}{\partial t} = -W(\hbar\omega), \quad (5)$$

so that

$$\alpha(\hbar\omega) = \sum_{ij} \frac{\pi\hbar^2 e^2}{m_0^2 \omega\varepsilon} |\langle k_j | a \cdot \nabla | k_i \rangle|^2 \delta(E_j - E_i - \hbar\omega)\{ f[E(k_i)] - f[E(k_j)]\}. \quad (6)$$

We now begin to calculate the optical absorption when a semiconductor quantum well sample is illuminated. By defining the growth direction of the sample as the z-axis, the plane perpendicular to this direction as the xy-plane, the Hamiltonian is

$$H = -\frac{\hbar^2 \nabla^2}{2m^*} + V(z), \quad (7)$$

in the effective-mass approximation, where m^* is the effective mass and $V(z)$ the quantum well potential energy. The interaction between the incident radiation and the electron is $e\hbar A \cdot \nabla / m^*$ for an incident light of $A = A_0 e^{-i\omega t}$[15].

Since H is translationally symmetric in the xy-plane, the wave function can be expressed as

$$\Phi_{jk}(r) = \phi_j(z)\, u(r)\, e^{ik\cdot b}. \quad (8)$$

where $u(r)$ is the Bloch function and $r = (b, z)$. For all values of j, $u(r)$ is the same, as intra-band transitions among sublevels are involved in the detector. $u(r)$ is approximated as k-independent. k and b are the wave vector and coordinate in the xy-plane, respectively. $\phi_j(z)$ is the envelope function and is normalized in the z direction. Between ground sublevel $|\Phi_{0q}\rangle$ and excited ones, it is easy to show that

$$\langle \Phi_{jk} | \frac{e\hbar}{m^*} A \cdot \nabla | \Phi_{0q}\rangle = \delta_{k,q} \frac{e\hbar A_z}{m^*} \langle \phi_j | \frac{\partial}{\partial z} | \phi_0 \rangle. \quad (9)$$

Eq. (9) indicates the momentum conservation in the xy-plane, and the transition is between the envelope functions in the z-direction.

Moreover, the most important result implicated by Eq. (9) is the condition about the optical coupling: The coupling of a radiation with the carriers inside a quantum well structure is not possible at a normal incident condition (the light propagates along the sample growth direction so that the component of the vector potential along this direction, A_z, is zero). Optical grating is therefore a necessity in many practical quantum-well-based photodecetor devices.

The probability of an electron optically excited from the ground sublevel to sublevel j becomes

$$W_j = \int \frac{2\,dq}{(2\pi)^2} \left| \frac{e\hbar A_z}{m^*} \langle \phi_j | \frac{\partial}{\partial z} | \phi_0 \rangle \right|^2 \frac{2e^2 \Gamma}{\hbar(\hbar^2\Omega_j^2 + \Gamma^2)} [f(E_{0q}) - f(E_{jq})], \quad (10)$$

where we have replaced the energy conservation of $\delta(E_j - E_i - \hbar\omega)$ by the lifetime Γ of electrons in excited states.

2 Optical coupling

The QWIP is n-type and has an optical active layer consisting of 50 periods of $Al_{0.3}Ga_{0.7}As$-GaAs multiple quantum wells (MQWs) along the z-direction. Each $Al_{0.3}Ga_{0.7}As$ barrier is 500 Å thick and the GaAs well 50 Å thick. The GaAs layer is Si-doped at a level of $5 \times 10^{17} cm^{-3}$. Doping levels in the cap and bottom layers are $2 \times 10^{18} cm^{-3}$. Typical I-V characteristics is presented in Fig. 1, where a linear relationship between the current and the external bias at the low bias regime (< 2V) is generally observed. The slope of the I-V curve decreases in the bias range (3～6 V) where we observe a kind of current saturation. The current increases drastically when the bias is larger than 7V. Asymmetric property of the I-V characteristics is indicated with respect to the polarity of the bias voltage. The current density is

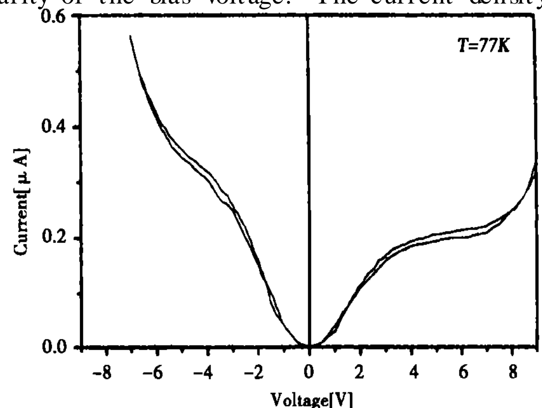

Fig. 1 Typical I-V characteristics of two optical pixels in one QWIP chip measured at 77 K

about 0.25mA/cm^2 at the saturation level.

The active Γ electrons are described by an effective mass of $m^* = 0.067\ m_0$ in GaAs layers and $0.091\ m_0$ in $Al_{0.3}Ga_{0.7}As$ barriers, where m_0 is the free electron mass. The conduction band offset is $0.65 \times 1.247x$ eV between $Al_xGa_{1-x}As$ and GaAs.

Due to the isotropic effective mass of the Γ electrons, normal incident photon absorption is not possible, as discussed in the last section. A component of the optical electric field along the QWIP growth direction, A_z is required. To utilize Γ electrons, diffraction gratings are needed for optical coupling. Electron-photon coupling, by Eq. (9), is achieved normally by a two-dimensional optical grating which is schematically depicted in Fig. 2. The diffraction grating structure consists of $2a \times 2a$ rectangular apertures, or circular apertures with radius a periodcally arranged on the optical pixel, at distance b from each other. The depth of the apertures is denoted as h. The right part of Fig. 2 shows the SEM picture of one grating obtained by wet etching technique.

The QWIP structure is not exactly nonconductive. However the current density at normal device working condition is very low so that the approximation of non-conduction with respect to the electromagnetic field is acceptable. When analyzing un-polarized infrared radiation, the vector nature of the wave amplitude will not be important, so that we can assume that we are dealing with a scalar amplitude function $\psi(r)$ which is a solution to the wave equation of [16]

$$\nabla^2\psi_{ph} + 4\pi^2 k^2\psi_{ph} = 0. \quad (11)$$

for purely elastic diffraction, where $2\pi k = \sqrt{\varepsilon\mu}\,\omega$ is the wave number. By Huygen's principle and considering a light source far away from the diffraction plane XY, the optical wave function for the refractive diffraction grating defined by its reflection coefficient $q(X, Y)$ which is perpendicular to the direction of radiation incidence, becomes [17,18]

$$\psi_{ph}(x, y, R) = \iint q(X, Y)\frac{e^{-i2\pi kr}}{r}\left(\frac{1}{r} + i2\pi k\cos\theta - i2\pi k\right)dXdY. \quad (12)$$

$r^2 = (x - X)^2 + (y - Y)^2 + R^2$, R is the distance from the observation plane xy to the diffraction grating plane XY. θ is the angle between the z axis and vector r.

For an incident radiation of $1/k = 8\mu m$ (in vacuum) and a reflective grating structure of $56 \times 56\mu m^2$ ($X, Y \in (-28, 28)\mu m$) ($a = 2$, $b = 8$, $h = 1.5$, $R = 2\mu m$, i.e., 7×7 apertures arranged in the form of Fig. 2, where R is the thickness of the top n^+ GaAs contact layer which separates the grating from the absorbing QWIP layer), the calculated electric field in the area of $(x, y) \in (0, 30)\mu m$ for square apertures is presented in Fig. 3a.

Periodicity is observed in the optical field ψ in the xy-plane which is determined by the wavelength of the incident radiation. Such a periodicity is expected when considering a one-dimensional grating structure so that the oscillation factor becomes $e^{-j2\pi kr} = e^{j2\pi kx}\cdot e^{-i2\pi kX}$. This is very much alike the so-called near-field effect which has been extensively applied to the surface properties [19]. In addition, fringing field effct (see Fig. 3a) for $x, y > 28\mu m$ is also very strong. The fringing field effect causes the cross talking between adjacent optical pixels on a FPA.

Knowing the distribution of the optical field, we can calculate the amplitudes of different optical plane

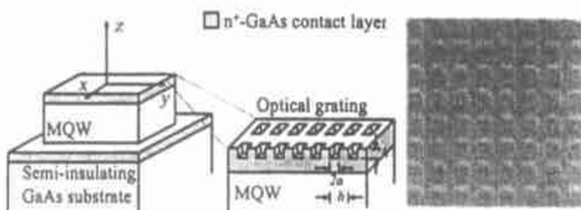

Fig. 2 Geometric structure of the two-dimensional optical grating for a GaAs/AlGaAs QWIP, and a SEM picture of grating (6-μm period and 0.6-μm depth) by wet etching technique

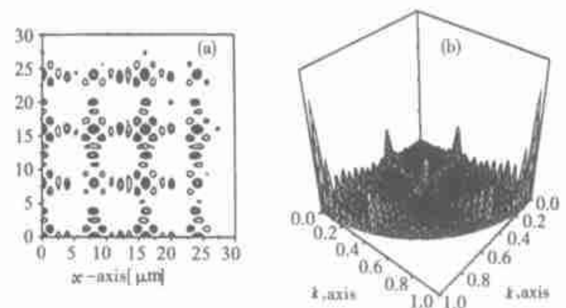

Fig. 3 (a) The spatial distribution of the diffracted electric field ( ) T f ff f f x and k_y in units of $k = 1/2.21[\mu m^{-1}]$

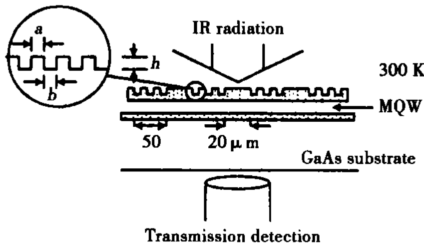

Fig. 4 Optical grating and experimental setup of the radiation transmission

waves propagating in different directions. The otical field can be expressed as

$$\psi_{ph}(x, y, z) = e^{i2\pi kz} + \sum_{k} t_k e^{i2\pi(k\cdot b - k_z z)}, \quad (13)$$

where $r = (b, z)$ and $e^{i2\pi kz}$ is the original incident radiation propagating along the z-direction, t_k is the amplitude of the plane wave propagates along the - z-direction with wave vector $k = (k_x, k_y)$ in the xy plane after diffraction. Since we consider only elastic scattering, $k_x^2 + k_y^2 + k_z^2 = k^2$.

The diffraction grating is to be designed for large values of t_k corresponding to small values of k_z. The larger can be these amplitudes, the larger will be the effective optical strength to excite optical transitions, and thus it can be produced that a larger optical coupling between the incident photons and active electrons in the QWIP. The amplitude of the diffraction radiation from our diffraction grating of Fig. 2 is shown in Fig. 3b. Defining the effective strength of the diffracted radiation along the z-direction which

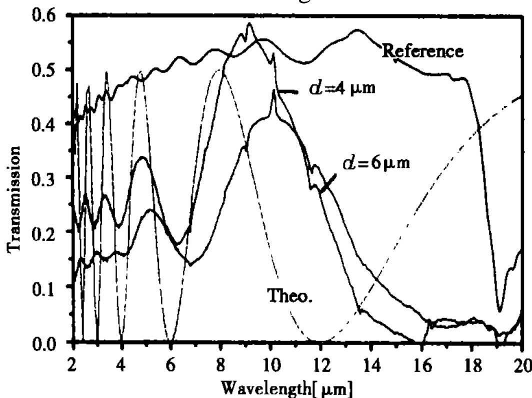

Fig. 5 Soild lines: transmission spectra of QWIPs ($h = 0.7\mu m$). Same results have been obtained for both normal and back illumination setups as well as for mesa-etched structures. Dotted line: the transmitted optical field strength

can absorbed by the Γ electrons in the GaAs quantum well as $\langle |A_z|^2 \rangle = A^2 B/2$, where A is the amplitude of the incident infrared radiation and the factor of 1/2 is due to the unpolarization of the incident radiation. The value of the B parameter for the grating structure of Fig. 3 is 0.6655. Similar results were reported earlier based on the EM mode approach[20].

Optical transmission spectrum of the infrared radiation (Fig. 4) is measured at room temperature to further analyze optical diffraction by the grating structure and radiation transmission in the MQW layer. The samples consist of 30 periods of GaAs/ $Al_{0.3}Ga_{0.7}As$ multiple quantum wells and the resultant transmission spectra are presented in Fig. 5 as functions of radiation wavelength, where the transitivity of the wafer (without grating) is in general about 50 %. Throught the gratings having periods of 4 and 6μm, the transmissions vary with the wavelength, whereas for 8-μm-period grating, a broader transmission valley is observed centered around 8-μm wavelength.

The fields due to the reflections at the two interfaces of the MQW active layer are $E_0 \sin(\omega t) + E_0 \sin(\omega t + \Phi)$, where the phase difference Φ depends on the path difference: $\Phi = 2\pi \times 2nl/\lambda$, where l is the thickness of the MQW layer (consisting of 30 periods of GaAs/AlGaAs quantum wells, $l = 1.65\mu m$) and $n = 3.65$ is the refractive index of the GaAs/AlGaAs MQW material. The transmission intensity of this field is

$$1 - \cos^2 \frac{\Phi}{2}, \quad (14)$$

which is presented in Fig. 5 as the dotted line. We have observed an excellent agreement between measurements and theoretical expectation.

In the forthcoming part we shall discuss the electrical aspects of the quantum well infrared photodetector.

REFERENCES

[1] Casselman T N. State of infrared photodetectors and materials. Proceedings of the SPIE, 2999:2—10

[2] Rogalski A. Comparison of the performance of quantum well and conventional bulk infrared photodetectors. Infrared Physics and Technology, 1997, 38:295—310

[3] Gunapala S D, Bandara S V, Liu J K, et al. Long-wavelength 640 ×486 GaAs/ AlGaAs quantum well infrared photodetector Snap-Shot camera. IEEE Transactions on Electron Devices, 1998, 45:1890—1895

[4] Levine B F. Quantum-well infrared photodetectors. J. Appl. Phys, 1993, 74:R1—81

[5] Wan M F, Ou H J, Lu W, et al. Infrared imaging by 128 ×1 GaAs/ AlGaAs MQW infrared FPAs. J. Infrared Millim. Waves (万明芳, 欧海疆, 陆卫, 等. 128 ×1 元 GaAs/ AlGaAs 多量子阱扫描型红外焦平面的红外成像. 红外与毫米波学报), 1998, 17:76—79

[6] Shen S C. Comparison and competition between MCT and QW structure material for use in IR detectors. Microelectronics Journal, 1994, 25:713—739

[7] Lu W, Ou H J, Chen M H, et al. Study on the practicality of GaAs/ AlGaAs muliple quantum well infrared detector. J. Infrared and Millimeter Waves (陆卫, 欧海江, 陈敏辉, 等. GaAs/ GaAlAs 量子阱红外探测器实用性探讨. 红外与毫米波学报), 1994, 13:9—13; Lu W, Ou H J, Chen M H, et al. Application of GaAs/ AlGaAs multiple-quantum well infrared detector array. International J. Infrared Millimeter Waves, 1994, 15:137—140

[8] Bratt P R, Casselman T N. Potential barriers in HgCdTe heterojunctions. J. Vac. Sci. Technol., 1985, A3:238—245

[9] Kosai KJ, et al. Status and application of HgCdTe device modeling (IR detectors). J. Electronic Materials, 1995, 24:635—640

[10] Helms C R, Melendez J L, Robinson H G, et al. Process simulation for HgCdTe infrared forcal plane array flexible manufacturing. J. Electronic Materials, 1995, 24:1137—1142

[11] Choi K Ked. The Physics of Quantum Well Infrared Photodetectors. Singapore: World Scientific Publishing Co. Pte. Ltd. 1997

[12] Fu Y, Willander M, Lu W, et al. Optical coupling in quantum well infrared photodetector by diffraction grating. J. Appl. Phys. 1998, 84:5750—5755

[13] Fu Y, Willander M, Lu W, et al. Near-field coupling effect in normal incidence absorption of quantum well infrared photodetectors. J. Appl. Phys. 1999, 85:1237—1239

[14] Fu Y, Li N, Karlsteen M, et al. Thermoexcited and photoexcited carrier transports in a GaAs/ AlGaAs quantum well infrared photodetector. J. Appl. Phys., 2000, 87:511—516

[15] Sze S M. Physics of Semiconductor Devios. 2nd Edition, New York: John Wiley & Sons, 1981, 32

[16] Kishino K, Arai S. Chapter 11 Integrated Lasers, Handbook of Semiconductor Lasers and Photonic Integrated Circuits. London: Chapman & Hall, 1994, 350

[17] Stover J C. Optical Scattering: Measurement and Analysis. New York: McGraw-Hill, 1990, 51

[18] Cowley J. Diffraction Physics. Elsevier Amsterdam, 1995, 11

[19] Barenz J, Eska A, Hollricher O, et al. Near-field luminescence measurements on GaInAsP/ InP double heterostructures at room temperature. Appl. Optics, 1998, 37:106—112

[20] Andersson J Y, Lundqvist L. Near-unity quantum efficiency of AlGaAs/ GaAs quantum well infrared detectors using a waveguide with a doubly periodic grating coupler. Appl. Phys. Lett., 1991, 59:857—859; Andersson J Y, Lundqvist L. Grating-coupled quantum-well infrared detectors: theory and performance. J. Appl. Phys., 1992, 71:3600—3610